PAPER

Check for updates

Magnetic and luminescent lanthanoid (Ln = Tb, Dy) 2D MOFs on functionalized silicon

Elena Bartolomé, [*a] Pablo Sevilla, [b] Guillem Gabarró-Riera, [c] Ana Arauzo, [d]
Juan Rubio Zuazo [ef] and E. Carolina Sañudo [*cg]

The controlled deposition of organized molecular materials on technologically relevant substrates is crucial for the development of innovative magneto-optical devices. In this work, we report the growth of lanthanoid-based 2D metal–organic frameworks (MOFs) with formula unit $[Ln(MeCOO)(PhCOO)_2]$ (Ln = Dy, Tb) on Si(100) wafers functionalized by silanization. The thickness, morphology and composition of the grown material was assessed using a combination of ellipsometry, contact angle measurements, scanning electron microscopy (SEM) and energy dispersive X-ray spectroscopy (EDS). The on-surface grown terbium 2D MOFs exhibit green luminescence, like the bulk. Furthermore, chemisorbed Dy and Tb 2D MOFs retain a significant magnetic moment, as demonstrated by X-ray magnetic circular dichroism (XMCD) measurements conducted at the $M_{4,5}$ edge of the two lanthanoids. Our work paves the way for the preparation of magneto-optical devices and organized arrays of single-molecule magnets (SMMs) and qubits on surfaces for high-density information storage and quantum computing applications.

Introduction

2D molecular materials are receiving growing interest due to their vast application potential in electronics, spintronics, energy storage, catalysis, sensing, biomedicine,[1] as well as the interesting new physics that emerge at the 2D limit.[2,3] Recent advances in coordination chemistry have enabled the synthesis of 2D metal–organic frameworks (2D MOFs), which can be conveniently functionalized.[4] This is a clear advantage over 2D inorganic materials like graphene or transition metal sulfides. Evidence of long-range ferromagnetic order in an atomically-thin and extended Fe metal–organic coordination network on Au(111) has been recently demonstrated.[5]

The investigation of 2D MOFs based on lanthanoids is particularly promising for obtaining arrays of single-molecule magnets (SMMs) for information storage or arrays of qubits for quantum information processing technologies. 2D MOF arrays of qubits can be designed so as to control dipolar interactions and magnetic dilution, which impact quantum decoherence, and to integrate qubits into devices.[6] Additionally, Ln(III) 2D MOFs offer processable materials for on-surface magnetic refrigeration leveraging the magnetocaloric effect (MCE),[7] and the development of multifunctional materials combining magnetism and luminescence for novel magneto-optical applications.[8–11]

The growth of molecular nanosheets like those of 2D MOFs on surfaces is a crucial step toward further manipulation of the material and fabrication of devices for these applications. However, the deposition of magnetic molecules on surfaces and the understanding molecule–substrate interactions are non-trivial.[12,13] Various approaches to deposit nanomagnet systems of increasing complexity on surfaces have been recently reviewed.[14–26]

In previous work, we reported the preparation of homometallic and heterometallic 2D MOFs using lanthanoid ions, with the general formula $[Ln(MeCOO)(PhCOO)_2]$. The Dy analogue displayed SMM properties, which were enhanced when the system was diluted with La:Dy 9:1.[10] The Tb and TbEu analogues exhibited both SMM and luminescent properties.[11] Separation between the 2D layers in the crystal is provided by weak van der Waals forces, allowing exfoliation by sonication

[a] *Institut de Ciència de Materials de Barcelona (ICMAB-CSIC), Campus UAB, 08193-Bellaterra, Barcelona, Spain. E-mail: ebartolome@icmab.es*

[b] *Escola Universitària Salesiana de Sarrià (EUSS), Passeig Sant Joan Bosco, 74, 08017-Barcelona, Spain*

[c] *Departament de Química Inorgànica i Orgànica, Universitat de Barcelona, C/Martí i Franqués 1-11, 08028 Barcelona, Spain. E-mail: esanudo@ub.edu*

[d] *Instituto de Nanociencia y Materiales de Aragón (INMA-CSIC) – Universidad de Zaragoza, Pedro Cerbuna, 12, 50009 – Zaragoza, Spain*

[e] *Spanish CRG Beamline BM25-SpLine at the ESRF, 71 Avenue des Martyrs, Grenoble 38043, France*

[f] *Instituto de Ciencia de Materiales de Madrid – Consejo Superior de Investigaciones Científicas (ICMM-CSIC), Sor Juana Inés de la Cruz, 3, Cantoblanco, Madrid 28049, Spain*

[g] *Institut de Nanociència i Nanotecnologia de l'Universitat de Barcelona IN2UB, C/Martí i Franqués 1-11, 08028 Barcelona, Spain*

This journal is © The Royal Society of Chemistry 2025

J. Mater. Chem. C, 2025, **13**, 21015–21026 | **21015**

into large nanosheets of average size 5 μm × 5 μm. Magnetic and luminescent Tb 2D MOF flakes were successfully deposited and characterized on various substrates such as silicon by spin-coating, and paper by drop-casting.[11,27]

Most efforts to integrate molecular materials onto surfaces have focused on the vapor deposition of suitable molecules that can be sublimated under ultra-high-vacuum (UHV) conditions like lanthanoid phthalocyanines,[15,16] vanadyl phthalocyanines,[17–19] Cr$_7$Ni qubits,[21–23] or Fe$_4$ SMMs.[24–26] However, in these instances, either isolated molecules or submonolayers of a few nm^2 are obtained, or a combination of both on the same substrate. Extension to broader areas might be of interest, and this could be achieved through chemical bonding between a functional group on the surface and the desired molecular system.

Silanization has been successfully utilized to functionalize *via* a chemical bond a wide variety of materials on oxidized substrates.[28–31] Triethylethoxysilanes can be obtained commercially with a variety of terminal groups, including a succinate group that hydrolyzes to afford two carboxylic acid groups. Surface functionalization with this type of silane results in a surface decorated with carboxylic acids, ideal for lanthanoid and transition metal chemistry.

Recently, we demonstrated that microcrystals of the Gd(III) complex [Gd(MeCOO)(PhCOO)$_2$] can be grown on silanized Si(100). Remarkably, the material retained its MCE properties in the surface-bound state, thus paving the way for on-surface magnetic refrigeration of devices at cryogenic temperatures.[32]

Furthermore, we employed a silanization strategy to achieve homogeneous deposition of monolayers of [Ln$_2$(SYML)$_3$(H$_2$O)] complexes (Ln = Eu(III), Dy(III); SYML = *N,N'*-bis(1-naphthaldi-amine)-*O*-phenylenediamine), featuring luminescent and magnetic properties, on large-area (1 cm × 1 cm) functionalized Si(100) substrates. Grazing incidence X-ray diffraction (GIXRD) measurements revealed preferred orientations and ordered domains of the chemically attached molecules.[33]

In this work, we report the growth of thin films of [Ln(MeCOO)(PhCOO)$_2$] (Ln = Tb, Dy) 2D MOFs on silicon wafers functionalized with carboxylic acid groups, and a detailed characterization of their on-surface structural, magnetic, and optical properties.[29]

Results and discussion

Chemisorption of crystallites of the 2D MOFs [Ln(MeCOO)-(PhCOO)$_2$] (Ln = Tb, Dy) onto functionalized Si wafers was achieved through the procedure schematized in Fig. 1, involving three steps: surface activation, functionalization and crystallite growth. A summary of the different studied samples is presented in Table 1.

Silanization of p-doped Si(100) with a suitable functionalized trialkoxysilane leads to **TSPSi**, a functionalized Si(100) substrate, bearing exposed carboxylic acid groups. These exposed carboxylic acid groups can easily react with lanthanoid ions to form a coordination bond, and thus enable the coordination of complexes chemically attached to the surface.
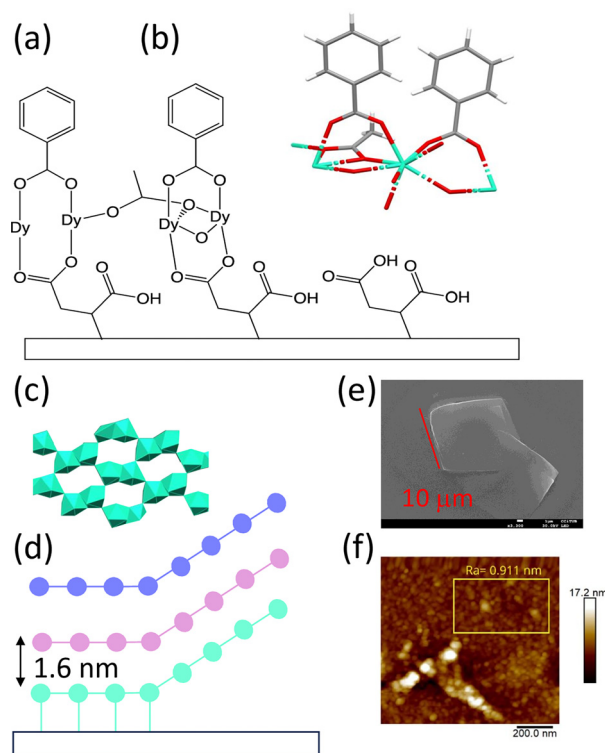

Fig. 1 Chemisorption process on functionalized **TSPSi**. (a) Schematic representation of functionalized **TSPSi** and the possible binding mode of the hydrolized succinate groups to dysprosium ions in the MOF; (b) crystal structure of **[Dy(MeCOO)(PhCOO)$_2$]** showing the binding modes of acetate and benzoato ligands. Dy green, oxygen red, carbon grey, hydrogen light grey. (c) Top view along the *z*-axis of the *xy*-plane of the hexagonal Dy(III) 2D layer in **[Dy(MeCOO)(PhCOO)$_2$]**, only the Dy(III) ions are shown for clarity. (d) Cartoon of **1DyTSPSi**, **1TbTSPSi** crystallites chemisorbed to **TSPSi**, resembling the SEM image in (e). The crystallite formed by three of these 2D layers (depicted in different colors) results of the van der Waals staking at 1.6 nm between 2D neutral layers, as observed in the crystal structure. Only a part of the first monolayer is chemisorbed. (e) SEM image of several crystallites chemisorbed to the **TSPSi** substrate in a sample of **1DyTSPSi**. (f) AFM image of some nanocrystallites for **1DyTSPSi**.

Alkoxysilane molecules with an organic functionality can be chemisorbed onto silicon surfaces following the procedure commonly known as silanization. Although this technique is widely employed for biomaterials functionalization, the characterization of silanized substrates remains challenging, and no consensus exists on the optimal conditions for obtaining self-assembled monolayers. Based on established protocols in the literature, we developed a protocol[33] that reproducibly affords a silicon substrate functionalized with carboxylato groups, which are necessary for the chemisorption of carboxylate-bridged coordination complexes, such as the reported 2D MOFs [Ln(MeCOO)(PhCOO)$_2$].

The silane selected for Si functionalization was [(3-triethoxy-silyl)propyl]succinic anhydride (TSP). This silane features three ethoxy groups that, after hydrolysis, can bond covalently with the Si atoms of the substrate. A three-carbon chain separates the silane silicon from the succinate group. In **TSPSi**, the succinate functional group can undergo hydrolysis resulting

21016 | *J. Mater. Chem. C*, 2025, **13**, 21015–21026

This journal is © The Royal Society of Chemistry 2025

Table 1 Summary of the studied samples. The table lists the sample codes, their composition, structural characteristics, and preparation conditions. Full synthetic details are provided in the Experimental methods section

Sample	Ln(III)	Characteristics	Growth conditions
TSPSi	—	p-doped Si(100) wafer functionalized with TSP	Ref. 33
[Dy(MeCOO)(PhCOO)$_2$]	Dy	Bulk Dy 2D MOF	Ref. 10
1DySi	Dy	2–10 nm Dy 2D MOF on non-silanized Si	1 h
1DyTSPSi	Dy	2–4 nm Dy 2D MOF on silanized Si	15–60′
2DyTSPSi	Dy	14 nm Dy 2D MOF film on silanized Si	1–24 h
3DyTSPSi	Dy	>30 nm thick, bulk-like sample on silanized Si	Non-diluted reaction mixture; 24 h
[Tb(MeCOO)(PhCOO)$_2$]	Tb	Bulk Tb 2D MOF	Ref. 27
1TbSi	Tb	∼5 nm Tb 2D MOF on non-silanized Si	24 h
1TbTSPSi	Tb	∼1 nm Tb 2D MOF on silanized Si	15–60′
2TbTSPSi	Tb	13.4 nm Tb 2D MOF film on silanized Si	1–24 h
2′TbTSPSi	Tb	15 nm Tb 2D MOF film on silanized Si	Non-diluted reaction mixture; 1 h

in two carboxylates, which can subsequently be used to react with lanthanoid ions.

The contact angle of **TSPSi** was typically 60°, indicating a more hydrophobic surface than that of the pristine (non-activated) Si(100) wafer (48°). This confirms complete coverage of the Si surface with a TSP monolayer. Furthermore, the typical silane layer thickness (∼0.9 nm) was consistent with previously reported values.

Chemisorption of [Ln(MeCOO)(PhCOO)$_2$] (Ln = Tb, Dy)[10,27] onto **TSPSi** was inspired by our previous results on chemisorbed molecular complexes.[33] We use a reaction mixture obtained from the microwave reactor after isolating a small quantity of precipitate. From these colorless solutions, plate-like crystals of [Ln(MeCOO)(PhCOO)$_2$] (Ln = Tb, Dy) can be obtained after *circa* one week. By immersing the functionalized **TSPSi** substrates in the reaction mixture, we expect some of the carboxylate ligands in [Ln(MeCOO)(PhCOO)$_2$] to be replaced by the surface carboxylate groups, thus yielding chemisorbed [Ln(MeCOO)(PhCOO)(RCOO)] (Ln = Tb, Dy) where RCOO are the surface carboxylate groups. The resulting samples are named **1DyTSPSi**, **1TbTSPSi**, **2DyTSPSi** and **2TbTSPSi**.

The crystal structure of the 2D MOFs for dysprosium[10] and terbium[27] has been described in detail elsewhere. The 2D layers are formed by Ln-acetato ligands, with benzoate ligands above and below the Ln-acetato 2D layer. The benzoato ligands are in the typical *syn,syn*-COO coordination mode bridging two lanthanoid ions perpendicular to the 2D monolayer, while the acetate ligands are part of the Ln–MeCOO-2D monolayer (Fig. 1b). The layers are stacked in a crystal by van der Waals interactions, with an interlayer spacing of 1.6 nm.

Initially, we hypothesized that chemisorption would involve the exchange of the benzoate ligands on one side of the monolayer by TSP carboxylates, as shown in Fig. 1a. However, our experiments showed that something else was happening, as crystallites were chemically attached to the surface even after short deposition times. A second possibility is that some acetato ligands at the edge of the 2D layer could serve as anchoring points for the TSP carboxylate groups. It is difficult to assess which of these options is happening, as both will entail subtle changes to the crystal field of a limited number of the lanthanoid ions of the sample.

As the first monolayer forms, *via* Ln-silane-COO coordination bonds, defects or boundaries facilitate the nucleation of crystallites that grow at an angle from the surface, as evidenced by SEM and AFM images. Changes in the number of crystallites, and their size can be affected by controlling the deposition times and the initial concentration of the solution. SEM images of these samples (Fig. 2a and Fig. S1.2) show that randomly oriented nano and microcrystallites are found on the surface, anchored to the substrate by a side or vertex. Thus, even at short deposition times, nanocrystals are found on the surface, above a homogenous, compact layer that has roughness higher than that of **TSPSi** (R_a (**TSPSi**) = 0.162 nm; R_a (**1DyTSPSi**) = 0.911 nm)) (see Fig. 1f and Fig. S1.3). After the deposition time, great care is taken in rinsing and cleaning the substrates from physiosorbed materials. This process includes sonication to effectively remove all non-chemisorbed nanocrystallites from **1DyTSPSi** and **1TbTSPSi**, **2DyTSPSi** and **2TbTSPSi**. With the same protocol but without the reaction mixture dilution step, we prepared after 24 h of immersion time the bulk-like sample **3DyTSPSi**, and after 1 h immersion, terbium sample **2′TbTSPSi**. SEM images are presented in Fig. 2 and Fig. S1.2. The difference between these samples is mainly the immersion time of the substrate, which results in thicker and less homogeneous coatings for longer deposition times (**1DyTSPSi** *vs.* **2DyTSPSi**), and in the indiscriminate growth of microcrystals on the surface for long immersion times in a non-diluted reaction mixture (**3DyTSPSi**).

SEM also allows us to understand the morphology of the surface. Clearly, SEM images of **1DyTSPSi**, **2DyTSPSi** in Fig. 2 show how microcrystallites of the MOF grow on the surface of the functionalized **TSPSi**, and how many of these crystallites grow in random orientations from the surface (see also SI, Fig. S1.2). These crystallites share the habit of the single crystals of the [Ln(MeCOO)(PhCOO)$_2$] (Ln = Tb, Dy) 2D MOFs used for SCXRD: they are thin square plates, very large in *xy*-plane (typically >5 μm) and very thin along the *z*-axis. In the *z*-directions, the 2D MOF layers are stacked by van der Waals forces, with a distance of 1.6 nm between the hexagonal layers of lanthanoid ions.

The silane layer serves a double purpose: first, it is a buffer organic, dielectric layer that isolates the magnetic 2D MOF layer from the substrate and second, it can help orient the growth of the crystallites of the magnetic material on the surface. In previous work with molecular SMMs, we were able to find

This journal is © The Royal Society of Chemistry 2025

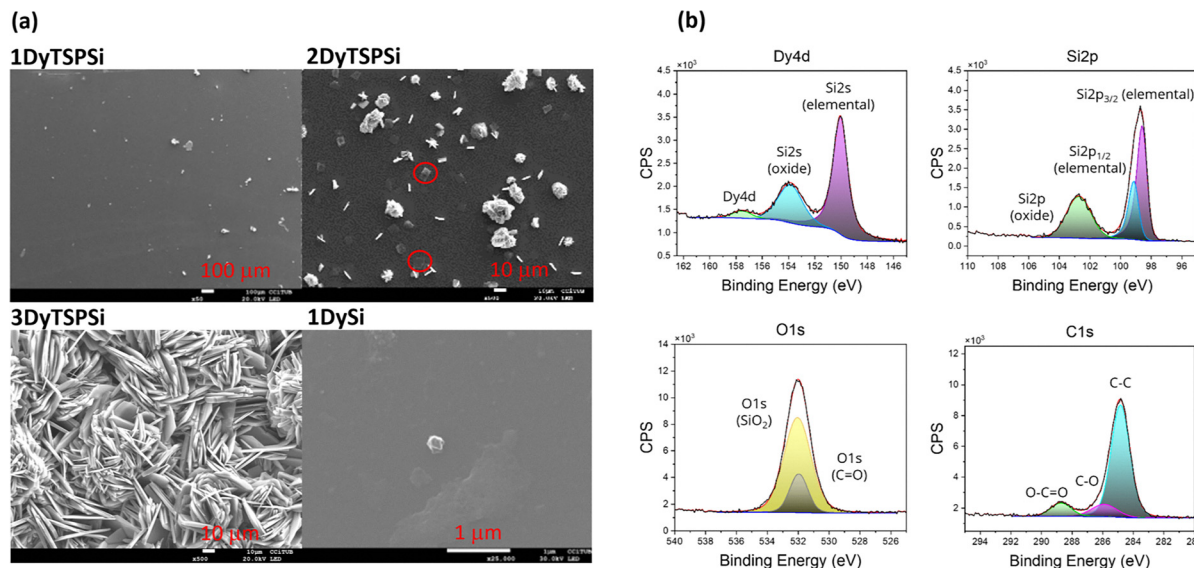*J. Mater. Chem. C*, 2025, **13**, 21015–21026 | **21017**

Fig. 2 (a) SEM characterization of samples **1DyTSPSi**, **2DyTSPSi**, **3DyTSPSi** and **1DySi**; (b) XPS analysis of **1DyTSPSi**. For full XPS survey spectra for all samples, see SI, Fig. S2.

ordered domains using functionalized **TSPSi**. This is a complex matter, since the silane has some flexibility and the layer can bear carboxylate groups that may not be perfectly ordered to the expected periodicity of the benzoato ligands in the monolayers of $[Ln(MeCOO)(PhCOO)_2]$. Our previous studies showed that the silane layer is compact but even so, only domains of ordered molecules were observed in 1×1 cm^2 samples.[33] Here, to provide insights onto the role of the silane layer, we used the same protocol to grow the 2D MOFs directly on activated bare **Si** substrates, producing the samples called **1DySi** and **1TbSi**. The rinsing and cleaning protocol, which includes sonication was also performed to remove any physiosorbed material. In these samples, some benzoato or terminal acetato ligands should be replaced by surface hydroxyl ligands if there is effective chemisorption. For the same deposition conditions, deposition times between 1–24 hours afforded average thicknesses between 4 to 10 nm—similar to values obtained for short deposition times (from minutes to 1 hour) on TSP Si samples (**1DyTSPSi** and **1TbTSPSi**). Therefore, it seems that the growth of chemisorbed crystals is possible on both TSP-functionalized silicon wafers and bare Si(100). In both cases, one has to consider the mismatch between the periodicity of the carboxylato groups from the 2D MOF and the possible binding sites (carboxylates in **TSPSi** and hydroxides in activated **Si**).

Contact angle measurements using the sessile drop method were performed to assess the hydrophilicity of the generated surfaces **1LnTSPSi** and **2LnTSPSi** (Ln = Dy, Tb). Chemisorption of $[Ln(MeCOO)(PhCOO)_2]$ is expected to result in a more hydrophobic surface compared to **TSPSi**, which is functionalized with succinate groups amenable to hydrolysis. The pristine commercial Si(100) wafers exhibited contact angles of approximately 40–50°. Activation using an arc-corona discharge or oxygen plasma yielded Si(100) surfaces that wet completely. Upon functionalization, typical contact angle values for **TSPSi**

were 60°, in agreement with a more hydrophobic surface. Typical values for **1LnTSPSi** and **2LnTSPSi** (Ln = Dy, Tb) were $68 \pm 4°$, indicating an even more hydrophobic surface, due to the replacement of the succinate groups of the silane by phenyl rings from the MOF. Typical contact angle images are shown in SI, Fig. S1.4.

The resultant thickness was measured using optical ellipsometry. Typical values for **1LnTSPSi** (immersion times between 15 to 60 minutes) were between 2 and 6 nm, while for **2LnTSPSi** (immersion times 1 to 6 hours) values of 10 to 18 nm were obtained. Ellipsometry results show that the thickness of the 2D MOF film increases with longer immersion times. It is important to note that the 1 mm diameter laser spot used in ellipsometry provides an average value over a very large area of the sample. Given the surface heterogeneity of the studied samples, the values obtained by ellipsometry represent an average across regions with only one monolayer and regions where nano- and microcrystals are clearly present, as shown by SEM and AFM images (Fig. 2 and Fig. S1.2, S1.3).

Qualitative information about the species present on the sample surface was obtained using Attenuated Total Reflection Infrared (ATR-IR) spectroscopy. Spectra for **1DyTSPSi** sample showed weak peaks that can be attributed to lanthanoid-coordinated carboxylate groups (see SI, Fig. S1.1).

The presence of the expected MOF and of Dy(III) at the sample surface was confirmed by SEM-EDS and XPS. EDS is a local elemental analysis technique, qualitative and with limited resolution. For **1DyTSPSi**, **2DyTSPSi** and **3DyTSPSi** dysprosium was detected using EDS. XPS offers higher sensitivity but yields a value averaged over a wide area of *ca.* 2 mm^2. XPS is a surface sensitive technique, based on detection of low energy electrons that must scape the sample. For thin samples as **1DyTSPSi**, an XPS spectrum should still display silicon peaks from the substrate. XPS spectra confirmed the expected elemental

21018 | *J. Mater. Chem. C*, 2025, **13**, 21015–21026

This journal is © The Royal Society of Chemistry 2025

composition of the nanometric layer and showed dysprosium, carbon, oxygen and silicon in **1DyTSPSi**. The high-resolution spectra of Dy 4d, Si 2p, C 1s and O 1s are shown in Fig. 2b. The Dy 4d peak appears at 157.5 eV, in agreement with dysprosium in the expected 3+ oxidation state and alongside the peaks for Si 2s (at 153.8 eV for SiO_2 and 150.0 eV for elemental silicon). The Si 2p region presents the expected peaks at 98.7 eV corresponding to the elemental Si $2p_{3/2}$ and Si $2p_{1/2}$ electrons, and at 102.7 eV corresponding to the SiO_2 native layer. The oxygen O 1s region presents a wide peak that can be deconvoluted into two peaks, corresponding to the SiO_2 layer and the oxygen bound to the carbon from the MOF benzoato and acetato ligands.

Finally, the C 1s region presents three peaks. The most intense is at 284.8 eV and corresponds to C–C carbon. At higher binding energies we observe a peak corresponding to C–O (285.9 eV) and to a carboxylato's O–C=O (288.7 eV) from the benzoato, acetato and the silane of the **1DyTSPSi**. XPS spectrum of **2DyTSPSi** and **3DyTSPSi** showed similar features, but a higher atomic percentage of dysprosium (see SI Fig. S1.2).

In summary, the combination of ellipsometry, contact angle, SEM-EDS and XPS techniques confirmed the presence of **[Dy(MeCOO)(PhCOO)₂]** 2D MOF, chemisorbed on the functionalized **TSPSi** for the nanometric **1DyTSPSi** and **2DyTSPSi** and also the thicker **3DyTSPSi**, and indicated an increase in the Dy content with increasing immersion time.

Profiting from the larger penetration depth of high kinetic energy electrons, hard X-ray photoemission spectroscopy (HAXPES) was done at the BM25 beamline, SpLine at ESRF on **1DyTSPSi** and **1DySi** samples to figure out possible chemical states at the buried interfaces. Fig. 3a shows the photoemission spectra for the Si 1s and Dy $2p_{1/2}$ core levels of the two samples. The silicon 1s peak shows two contributions in both samples. The dominant peak in **1DySi** has a binding energy of 1839 eV corresponding to Si^0 whereas the dominant peak in **1DyTSPSi** has a binding energy of 1844 eV corresponding to SiO_2. This effect can be ascribed to the matching of the HAXPES penetration depth to the stacking thickness in order to see interfacial effects. The silane layer on **1DySiTSP** increases the total stacking thickness maximizing the signal from the underneath SiO_2 layer, as sketched in Fig. 3a. However, the absence of silane

layer on **1DySi** maximizes the signal from the buried Si substrate. The observed HAXPES $2p_{1/2}$ peak for Dy appears at 8585 eV for the **1DySiTSP** and **1DySi** samples. In both samples, the observed HAXPES $2p_{1/2}$ peak for Dy is displaced from the value expected for metallic dysprosium (8581 eV) to 8585 eV. The shift can be attributed to the oxidation state of Dy(III) in the 2D MOF (Dy(III) *vs.* Dy metal).

In order to monitor the chemisorption of Ln-2DMOF on top of the functionalized Si using photoluminescence, we prepared the samples also using Tb(III). This yielded samples **1TbTSPSi**, **2TbTSPSi** and **2′TbTSPSi**, analogous to the Dy counterparts. Fig. 4a compares the emission spectra obtained upon ligand excitation (λ_{exc} = 280 nm) for Tb 2D MOF/TSP/Si samples prepared using diluted and non-diluted reaction mixtures, and two different growth times (1 h, 24 h). To study the effect of the silanized layer, we also measured **1TbSi** prepared on non-silanized substrates. All spectra display the expected peaks for Tb(III) associated to $^5D_4$ to ^7F_J (J = 6, 5, 4, 3) transitions. The peak of maximum intensity corresponds to the $^5D_4 \rightarrow {}^7F_5$ transition at 544.9 nm. Fig. 4b shows the correlation between the intensity of this peak and the thickness of the grown 2D MOF material, determined from ellipsometry measurements. Results indicate that the largest luminescence intensity and thickness correspond to the sample **2′TbTSPSi**, prepared using a non-diluted reaction mixture and an immersion time of 1 hour. All samples prepared using a diluted reaction mixture (**1TbTSPSi**, **2TbTSPSi** and **1TbSi**) show a good correlation between the immersion time, layer thickness and luminescence intensity signals.

Magnetic properties of Ln 2D MOFs on TSP/Si

Surface-sensitive synchrotron radiation XAS-XMCD technique was used to investigate the magnetic properties of the thin (2–4 nm) Ln 2D MOFs chemisorbed on **TSPSi**, denoted **1LnTSPSi** (Ln = Dy, Tb). For comparison purposes, we characterized as well a sample without TSP, **1DySi**, and a 14 nm-thick MOF sample (**2DyTSPSi**). Additionally, we conducted measurements on powdered bulk samples of [Ln(MeCOO)(PhCOO)₂] (Ln = Dy, Tb) 2D MOFs, as a reference. The magnetic properties of **3DyTSPSi**, a thick (>30 nm) bulk-like grafted samples was carried on by standard SQUID magnetometry, and were coincident with those previously reported for the bulk material (see Fig. S3).
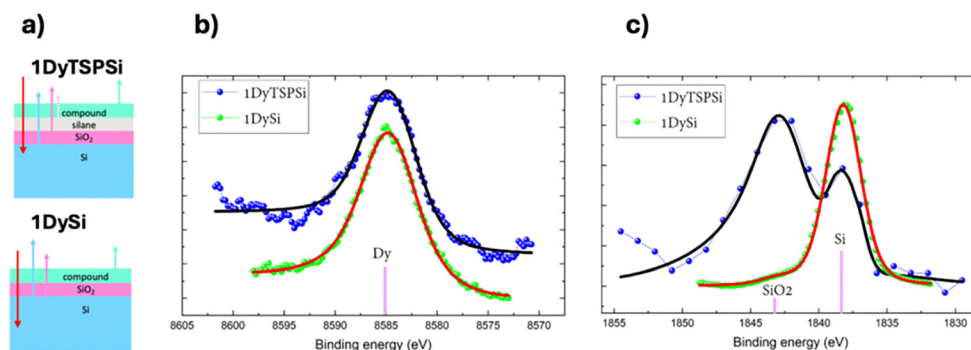

Fig. 3 (a) Cartoon of the profile of the **1DyTSPSi** and **1DySi** samples, with a red arrow indicating the penetration of X-rays (not to scale). HAXPES spectra for the (b) dysprosium and (c) silicon core levels of **1DyTSPSi** (blue scatter, black trace fitting) and **1DySi** (green scatter, red trace fitting).
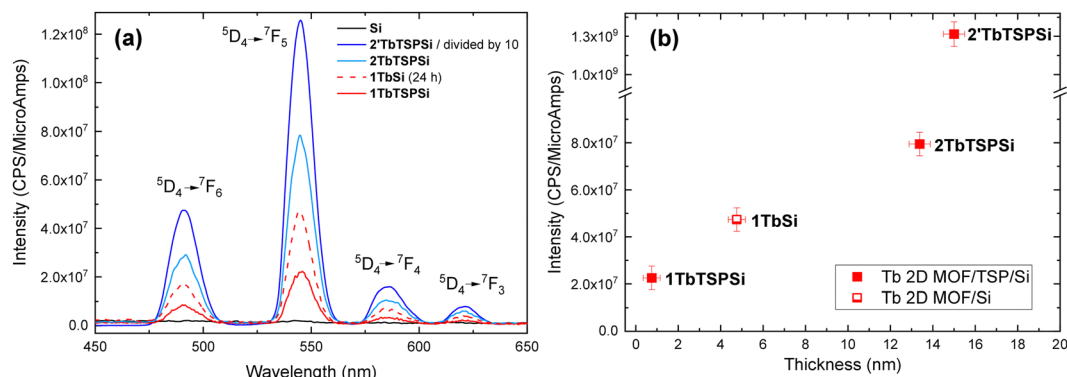
Fig. 4 (a) Luminescence emission spectra at excitation λ_{exc} = 280 nm for a series of Tb 2D MOF samples chemisorbed on TSP/Si (**1TbTSPSi**, **2TbTSPSi** and **2'TbTSPSi**) and, for comparison, the spectrum for Tb 2D MOF on non-silanized substrate, **1TbSi** (dotted line); (b) correlation between the intensity of the main $^5D_4 \rightarrow {}^7F_5$ peak and 2D MOF thickness obtained by ellipsometry.

The XAS-XMCD spectra measured for **1DySiTSP** at the Dy $M_{4,5}$ edge, and **1TbTSPSi** at the Tb $M_{4,5}$ edge, at 3.4 K, 6 T and normal beam incidence ($\theta = 0°$), as shown in Fig. 5a and b respectively, demonstrate the magnetic behavior of the chemisorbed 2D MOFs. Fig. 5a shows that the XAS-XMCD spectra at the Dy $M_{4,5}$ edge for the on-surface chemisorbed samples (*e.g.* **1DyTSPSi**, the non-silanized **1DySi**, and **2DyTSPSi**) and the powdered **[Dy(MeCOO)(PhCOO)$_2$]** bulk show a similar lineshape, coinciding with that expected for Dy^{3+} ions. The XAS spectra exhibits a main M_5 peak at 1295.96 eV with two pre-peaks at 1291.88, 1294.12 eV and a bulge at 1298.32 eV and two close features at M_4 1329.58, 1330 eV. The XMCD shows a main negative peak at M_5 1295.96 eV, a bulge at 1298.22 eV and positive peak at 1329.17 eV.

Likewise, the XAS-XMCD measured at the Tb $M_{4,5}$ edge for the chemisorbed **1TbTSPSi** and **[Tb(MeCOO)(PhCOO)$_2$]** bulk

powder (Fig. 5b) exhibit the expected lineshape for Tb^{3+} ions: the XAS spectrum presents a pre-peak at 1236.41 eV, a double-peaked M_5 (1239.37 eV, 1240.48 eV) and M_4 edge with a main peak at 1271.92 eV and a smaller one at 1274.54 eV. The XMCD spectrum displays a large, negative M_5 peak at 1240.54 eV and post-peak at 1243.50 eV, and three features at M_4 edge (1271.06, 1272.08, 1274.69 eV).

The small differences in the lineshape of the XAS spectra can be attributed to small changes in the coordination environment of some of the lanthanoid ions upon chemisorption, as illustrated in Fig. 1a. For the thinner samples (**1DyTSPSi** and **2TbTSPSi**) the number of lanthanoid ions affected should be larger and the lineshape differences bigger.

Magnetic anisotropy was further investigated on Dy samples. We measured the XAS-XMCD spectra at the Dy $M_{4,5}$ edge

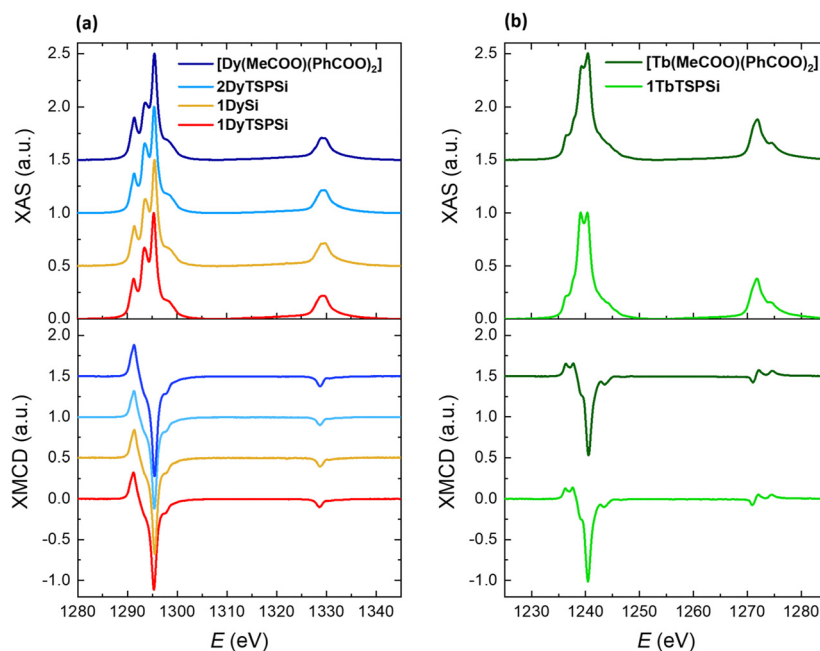**Fig. 5** Background subtracted, normalized XAS – XMCD spectra at 6 T, 3.4 K for $\theta = 0°$ beam incidence, (a) at Dy $M_{4,5}$ edge, for **1DyTSPSi**, non-silanized **1DySi**, the thicker **2DyTSPSi** sample and **[Dy(MeCOO)(PhCOO)$_2$]** bulk; (b) at Tb $M_{4,5}$ edge, for **1TbTSPSi** and **[Tb(MeCOO)(PhCOO)$_2$]** bulk.

21020 | *J. Mater. Chem. C*, 2025, **13**, 21015–21026

This journal is © The Royal Society of Chemistry 2025

at $\mu_0 H$ = 6 T and T = 3.4 K, as a function of the beam incidence angle (θ), varying between θ = 0° (normal incidence) to θ = 70° (grazing incidence), for **1DyTSPSi**, non silanized **1DySi**, and **2DyTSPSi** (Fig. S4). The orbital (m_L), spin (m_s) and total magnetic moment ($m_{TOT} = m_L + m_s$) per Dy(III) ion at each incident angle θ were determined from the XAS-XMCD spectra using the corrected sum rules for lanthanoids. Fig. 6 compares the $m_L(\theta)$, $m_s(\theta)$ and $m_{TOT}(\theta)$ angular dependence obtained for these three studied samples. The field-dependence of the total magnetic moment, m_{TOT}/ion(θ), determined for **1DyTSPSi** (Fig. 6a) exhibits a smooth angular dependence, reaching a maximum of m_{TOT} = 4.14 $\pm$ 0.02μ_B/ion at $\theta \approx$ 55°. This angular dependence could be modeled assuming the total magnetic moment arises from a 10% contribution of Dy ions pertaining to the thin layer with their Easy Axis of Magnetization (EAM) oriented at an angle β = 55° with respect to the substrate normal, and a 90% isotropic contribution from Dy microcrystallites deposited on the sample surface.

In contrast, **1DySi** exhibits a different m_{TOT}/ion(θ) angular dependence (Fig. 6b). The total magnetic moment reaches a maximum of m_{TOT} = 4.41 $\pm$ 0.02μ_B/ion at $\theta \approx$ 15° and decreases gradually with increasing the beam incidence angle, reaching m_{TOT} = 3.97 $\pm$ 0.02μ_B/ion at θ = 70°. This smooth anisotropic angular dependence may be explained by a linear combination of Dy ions in the Si-deposited thin layer, with their EAM forming an angle of β = 15° with respect to the substrate normal, and a 90% isotropic contribution from Dy microcrystallites.

In the case of the thicker **2DyTSPSi** sample, the determined m_{TOT}/ion(θ) shows a very weak angular dependence (Fig. 6c),

with m_{TOT} = 4.24 $\pm$ 0.02μ_B/ion at $\theta \approx$ 0°, and contains a predominantly isotropic contribution. Note measurements were conducted in TEY mode, which is only sensitive to the top 6 nm of the sample. Thus, given that this sample is 14 nm thick, the data primarily reflect the properties of its surface

In addition, the field dependence of the magnetic moment for these three samples was investigated by following the XMCD(H) at the Dy M$_5$ peak between −6 T and 6 T. The $m_{TOT}(H)$ curve was determined by normalizing the XMCD a.u. signal to the m_{TOT} value at 6 T, as obtained from the sum rules. Fig. 7 shows the $m_{TOT}(H)$ curves obtained at 3.4 K for **1DyTSPSi**, non-silanized **1DySi**, and **2DyTSPSi** in normal (θ = 0°) and grazing (θ = 70°) beam incidence. For comparison, Fig. 7c shows the $m_{TOT}(H)$ curve determined at the same temperature for **Dy** powdered sample. For the bulk, the experimental $m_{TOT}(H)$ is in good agreement with the predicted curve calculated using "Phi"[32] software at 3.4 K, with gyromagnetic tensor components g_x^* = 0.007, g_y^* = 0.020 and g_z^* = 19.281, previously calculated by *ab initio*,[10] and negligible interactions. For on-surface samples, the $m_{TOT}(H)$ curves are smoother and fall about 12% below that of the bulk. This result is in agreement with the illustration in Fig. 1, where we suggest a modification of the crystal field of Dy ions in 2D MOFs upon chemisorption on the surface. Nonetheless, a significant on-surface magnetic moment of m_{TOT} = 4.06, 4.31 and 4.23 μ_B/ion for **1DyTSPSi**, **1DySi** and **2DyTSPSi**, respectively, under θ = 0° beam incidence, is maintained. Anisotropy effects are small and most discernible for the **1DySi** sample, a thin 4–6 nm sample on non-silanized Si, as seen from previous XMCD(θ) experiments shown in Fig. 6.
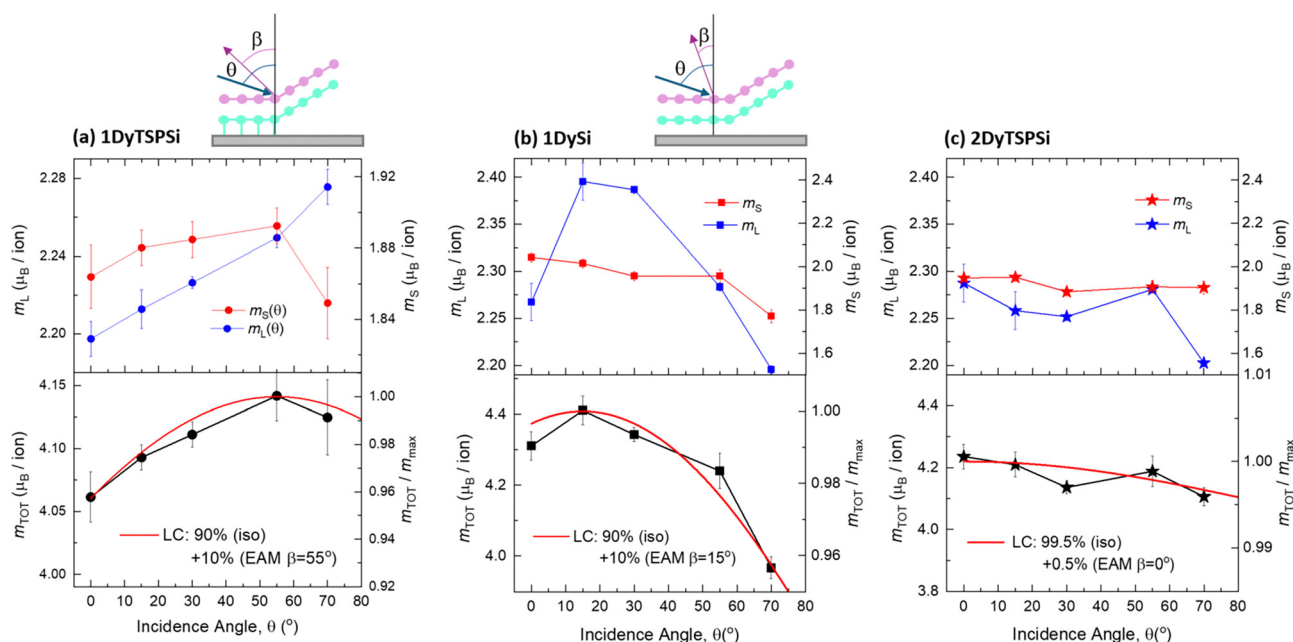

Fig. 6 Dependence of the orbital (m_L), spin (m_s) and total magnetic moments (m_{TOT}) with the beam incidence angle (θ), determined at 6 T and 3.4 K at the Dy M$_{4,5}$ edge, for (a) **1DyTSPSi**, (b) non-silanized **1DySi**, and (c) thicker **2DyTSPSi**. The angular dependence of the normalized magnetic moment was modeled as a linear combination (LC) of an isotropic contribution, associated to Dy bulk microcrystallites, and an anisotropic contribution owing to Dy ions in the layered 2D MOF with their easy axes of magnetization (EAM) oriented at an angle β with respect to the substrate normal: m_{TOT}/m_{max} ion(θ) = (%iso) + (%ani)·cos(θ − β).

This journal is © The Royal Society of Chemistry 2025

J. Mater. Chem. C, 2025, **13**, 21015–21026 | **21021**

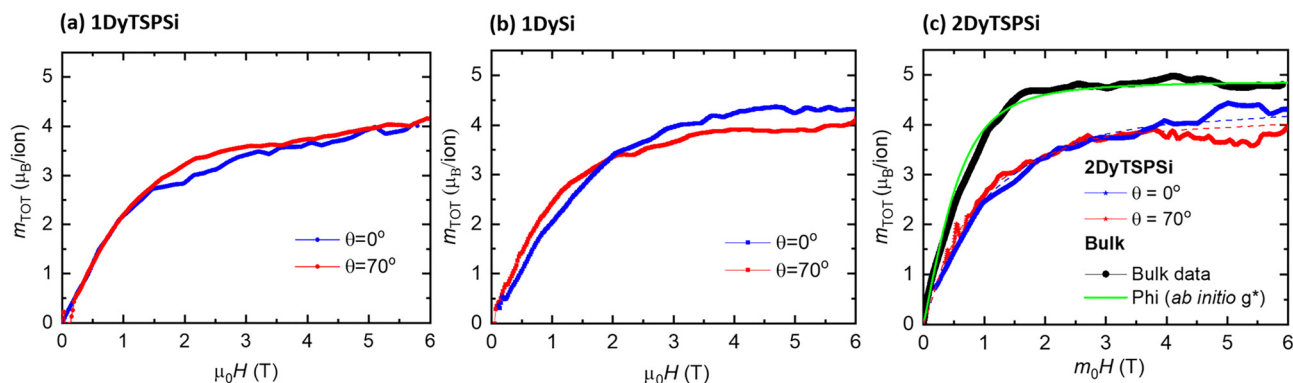**Fig. 7** Field dependence of the total magnetic moment, $m_{TOT}(H)$, at $T = 3.4$ K for (a) **1DyTSPSi**, (b) non-silanized **1DySi**, and (c) thick **2DyTSPSi**, in normal beam incidence $\theta = 0°$ (blue symbols), and grazing incidence, $\theta = 70°$ (red symbols). Fig. 7c also shows $m_{TOT}(H)$ measured for **Dy** bulk powdered sample, and (green line) theoretical prediction calculated using "Phi" software at 3.4 K with *ab initio*-calculated components of the gyromagnetic tensor $g\star$ $\left(g_x^* = 0.007, g_y^* = 0.020, g_z^* = 19.281\right)$ and negligible interactions.

Finally, to further investigate the formation of chemisorbed Dy 2D MOF material, we investigated XAS spectra using vertically (V) and horizontally polarized light (H), with respect to the synchrotron ring plane, at the O K edge, under grazing incidence ($\theta = 70°$) and zero applied field. The electric field vector E of linearly polarized X-ray acts as a "searchlight" for the valence band empty states in different directions of the atomic volume. For the selected experimental geometry, E_V lies in the sample substrate plane for V, while E_H is mostly out of plane (see Fig. 8 inset).

Fig. 8 compares the linear XAS spectra measured for **TSPSi** silanized substrate, **1DySi**, **1DyTSPSi**, and **2DyTSPSi**. In TEY mode, the penetration of X-rays is approximately 6 nm. The samples have the structure shown in the cartoon of Fig. 3: a nanometric layer of native silicon oxide on silicon crystal (pink SiO_2, blue Si) and a monolayer of silane (**TSP**, grey) for **TSPSi**;
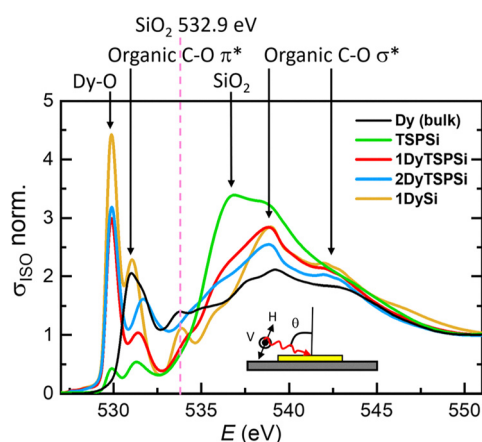

Fig. 8 Isotropic linear XAS, defined as $\sigma_{ISO} = (\sigma_{\parallel} + 2\sigma_{\perp})/3$, with $\sigma_V = \sigma_{\perp}$, and $\sigma_H = (\sin^2\theta)\sigma_{\parallel} + (\cos^2\theta)\sigma_{\perp}$ measured at the O K edge at $T = 3.4$ K, $H = 0$ and $\theta = 70°$, for silanized substrate (**TSPSi**), thin 2D MOF on non-silanized susbtrate (**1DySi**), thin 2D MOF on functionalized Si (**1DyTSPSi**), 14 nm **2DyTSPSi** and bulk, as reference. Inset: Sketch of the experimental configuration; H is parallel to the synchrotron ring plane, and V perpendicular to it.

1DyTSPSi and **2DyTSPSi** have the same profile, but with a few nm (**1DyTSPSi**) or 14 nm (**2DyTSPSi**) of 2D MOF (cyan). **1DySi** has a similar profile without the TSP silane layer. The clean functionalized wafer, **TSPSi**, should display the absorptions expected for the promotion of an electron from O 1s to the $\pi\star$ (532.3–532.5 eV) and $\sigma\star$ (542–549 eV) antibonding orbitals for the silane succinate group and the O 1s from silicon oxide (532.9 and 540 to 555 eV, broad poorly defined absorption bands). The absorption spectra observed for the silanized wafer is in agreement with the expected for a monolayer of TSP on the native SiO_2 layer on a Si crystal. One must consider that without the MOF, most of the electrons measured come from SiO_2 layer and silane (a total thickness of approximately 4 nm). Thus, as the MOF thickness grows from **1DyTSPSi** to **2DyTSPSi** the broad absorption of SiO_2 becomes less important. The features observed are in agreement with O 1s absorptions from SiO_2 and oxygen from organic compounds, Si–O–C and carboxylate groups

Table 2 summarizes the peaks observed in the O 1s linear XAS spectra, and their assignement, based on the known energies for different oxygen species, listed in the table as expected values.[34,35]

The bulk **[Dy(MeCOO)(PhCOO)$_2$]** MOF (see Fig. 8, black line) shows a complex absorption spectra for O 1s. Several absorption bands are observed of different intensities. The features observed are in agreement with a compound that contains O–Dy(III) bonds and organic carboxylate ligands coordinated to Dy(III). The spectrum shows a main feature at approximately 532 eV, a much weaker absorption at *ca.* 533 eV and broader features at higher energies.

In the samples where Dy 2D MOF has been chemisorbed on the functionalized silicon wafer, (**1DyTSPSi** and **2DyTSPSi**) there is a clear overlap between the absorption expected due to the promotion of an electron from O 1s to the $\pi\star$ (532.3–532.5 eV) and $\sigma\star$ (542–549 eV) antibonding orbitals for the organic ligands (benzoate and acetate), the silane succinate group and the absorptions reported for oxygen bonded to Dy(III). For heptacoordinated Dy(III) oxide the main features are O 1s → 5d-π (531.9 eV); d O 1s → 6p C (533.0 eV) and O

21022 | *J. Mater. Chem. C*, 2025, **13**, 21015–21026

This journal is © The Royal Society of Chemistry 2025

Table 2 Peaks observed in the O K-edge linear XAS spectra of the silanized substrate (**TSPSi**), 2D MOF on non-silanized susbtrate (**1DySi**), 2D MOF on functionalized Si (**1DyTSPSi** and **2DyTSPSi**), as shown in Fig. 8. Also, expected peak values for different oxygen species, according to ref. 34 and 35

	TSPSi	1DySi	1DyTSPSi	2DyTSPSi	Expected (eV)
Metal oxide		A	A	A	529–530
π* COO, COOH	B	B	B	B	532.3–532.5
σ* COO, COOH	E, F	E, F	E, F	E, F	542–549
O-Dy		B, C, C′	B, C, C′	B, C, C′	531.9, 533.0, 535.2
SiO$_2$	D	D	D	D	532.9, 540–555

$1s \rightarrow 5d$-σ 535.2 eV. In all samples **1DyTSPSi**, **2DyTSPSi** and **1DySi**, the Dy(III) ion is octacoordinated in a distorted square antiprism geometry. The energy for the promotion of an O 1s electron to an orbital with some Dy character will be in the same energy region as for the oxides, with expected changes and a complex structure of the O 1s signal. In the 2D MOF there are oxygen atoms from acetate coordinated to two Dy(III) ions, as well as oxygen atoms form benzoate ligands that are only coordinated to one Dy(III) ion.

We expect slightly different energies for the O 1s absorption for each of these cases. When the MOF is chemisorbed onto the succinate functionalized **TSPSi**, (**1DyTSPSi** and **2DyTSPSi**) the O 1s absorptions spectra should be complex, and we would expect a combination of the **TSPSi** and bulk MOF spectra. In fact, this is what we observed. For longer deposition times, in the **2DyTSPSi** sample we attain a thicker layer of 2D MOF chemisorbed on the **TSPSi**, consisting of large, micrometer-sized crystallites with various orientations with respect to the surface.

The O 1s X-ray absorption spectra is similar to the bulk MOF, with some features from the **TSPSi** substrate. The main difference is an intense peak observed at 530.8 eV (A). The intensity of this peak changes with the thickness of the 2D MOF film, being less intense for thicker samples. This matches the O 1s absorption of some metal oxides.[35] The absorption appears in all samples where the MOF is chemisorbed on silicon, but its intensity is reduced for the thicker **2DyTSPSi**. For the sample **1DySi**, without a silane to effectively chemisorb the MOF to the silicon wafer the absorption spectra for O 1s displays the features expected for the bulk MOF and those of the native SiO$_2$ layer, with a more pronounced peak of O 1s in SiO$_2$ at 532.9 eV.

Conclusions

Our study highlights the controlled growth of nanometric films of dysprosium and terbium 2D MOFs on Si(100) substrates functionalized with triethoxysilylpropyl succinic anhydride (TSP) by chemisorption. Within some limits, we can tailor the thickness and morphology of the chemisorbed material, as evidenced by comprehensive sample characterization employing ellipsometry, contact angle, SEM-EDS, and XPS techniques. Short immersion times (from minutes to 1 hour) of **TSPSi** in a diluted reaction mixture lead to films of average thicknesses between 2 to 6 nm in samples **1LnTSPSi** (Ln = Dy, Tb). Longer

immersion times (from 1 h to 24 hours) lead to thicker, 10–20 nm, samples **2LnTSPSi** (Ln = Dy, Tb). Using non diluted reaction times and longer deposition times we can obtain bulk-like films consisting of randomly oriented crystallites **3DyTSPSi**. Similar experiments were performed on pristine Si(100). The material can also be chemically attached to Si(100) (samples **1DySi**, **1TbSi**).

The grown thickness can be easily monitored by ellipsometry or by photoluminescence, in the case of terbium, exploiting the green luminescence of the bulk material which is not lost while grafted on a surface. This is an easy way to track the growth of chemisorbed 2D MOFs on functionalized and non-functionalized Si(100) wafers.

Moreover, our surface-sensitive XAS-XMCD measurements shed light on the on-surface magnetic properties of the Ln 2D MOFs (Ln = Dy, Tb) at 3.4 K and 6 T. Despite the total magnetic moment of Ln(III) ions in **1LnTSPSi** (Ln = Dy, Tb) is reduced about a 12% with respect to the bulk, a significant moment is retained. XAS-XMCD measurements performed as a function of the beam incidence angle for **1DyTSPSi** reveal a very weak angular dependence, which may be explained by an anisotropic contribution from Dy(III) ions within the first monolayer, aligned with their EAM at approximately $\beta = 55°$ from the substrate normal, and a predominant isotropic fraction originating from randomly oriented microcrystallites, as observed in SEM images. In contrast, for **1DySi**, a sample of similar thickness directly on Si(100) exhibits a weak, out-of-plane anisotropy ($\beta = 15°$), this might be attributed to a better alignment between the activated Si(100) anchoring points and the 2D MOF than for the **TSPSi** substrate carboxylate functional groups. The 14 nm-thick sample **2DyTSPSi** displays virtually no anisotropy. The results highlight the importance of considering not only the nature of the anchoring points in a functionalized substrate, but also the distribution of these, their orientation with respect to the surface and the crystal structure of the deposited 2D material.

Furthermore, **1DyTSPSi** and **2DyTSPSi** samples exhibited a smoother dependence on the magnetic field compared to the bulk, suggesting a modification of the crystal field and/or inter-ion interactions upon deposition, which is expected due to the proposed chemisorption. The presence of the silane layer fails to direct or impart order on the chemisorbed 2D MOF. However, comparing the thicknesses and luminescence of samples grown onto functionalized **TSPSi** and bare Si(100) we show that the silane layer helps in facilitating the growth of the 2D MOF on the substrate. This can be attributed to the fact that carboxylato groups are better ligands for the targeted material than the free hydroxyl that can be found in the activated Si(100) wafer.

Overall, the ability to chemisorb Dy and Tb 2D MOFs on technical substrates like silicon opens up exciting possibilities for the development of magneto-optical devices for various technological applications. Specifically, our findings offer promising avenues for organizing arrays of single-molecule magnets (SMMs) and qubits on surfaces, facilitating high-density information storage and quantum computing applications.

This journal is © The Royal Society of Chemistry 2025

J. Mater. Chem. C, 2025, **13**, 21015–21026 | **21023**

Importantly, magnetic dilution—crucial to mitigate decoherence in quantum devices—is achievable within our carboxylate 2D MOFs, as already demonstrated by the substitution of Dy with diamagnetic La.

Experimental methods

All chemicals were obtained from commercial sources and used as received without further purification. The silane [[(3-triethoxysilyl)propyl]succinic anhydride (TSP) was kept in a dry environment. The synthesis of $[Ln(CH_3COO)(PhCOO)_2]$ (Ln = Dy, Tb) was performed following the synthesis reported by our group for dysprosium[10] and terbium.[27]

Synthesis of $[Ln(CH_3COO)(PhCOO)_2]$ (Ln = Dy and Tb)

The bulk Dy(III) and Tb(III) compounds reported in this study were prepared following a previously reported procedure.[10,27] In brief, hydrated $Dy(MeCOO)_3 \cdot xH_2O$ or $Tb(MeCOO)_3 \cdot xH_2O$ was reacted with benzoic acid in a 1:2 molar ratio in a 1:1 methanol/acetonitrile mixture in a microwave reactor at 125 °C for 10 min with a pulse of 150 W. After cooling, a precipitate was removed by filtration, and the solution was left at 40 °C for several days, yielding colorless crystals of the corresponding 2D MOFs, ($[Dy(MeCOO)(PhCOO)_2]_n$ in 29% yield and $[Tb(MeCOO)(PhCOO)_2]_n$ in 37% yield.

Si(100) functionalized with [[(3-triethoxysilyl)propyl]succinic anhydride (TSPSi)

Details of this procedure were reported previously.[33] Single-side polished p-type Si(100) wafers were first activated with a plasma arc-corona treatment and sequentially cleaned in an ultrasonic bath using ethanol, 2-propanol, distilled water, and acetone (2 min each), followed by drying under nitrogen. The wafers were then transferred into 8 mL of toluene and heated to 80 °C under nitrogen. [[(3-Triethoxysilyl)propyl]succinic anhydride (TSP, >93%, TCI) was added (16 μL) and allowed to react for 15 min. Functionalized wafers (**TSPSi**) were sonicated in toluene, dried under nitrogen, and cured at 120 °C for 30 min under vacuum. A final cleaning sequence in ethanol, 2-propanol, and acetone (2 min each) was performed, followed by drying with nitrogen. The silane layer was characterized by ellipsometry (≈ 1.0 nm) and contact angle measurements ($\approx 60°$), confirming successful functionalization.

Growth of $[Ln(CH_3COO)(PhCOO)_2]$ on TSPSi (1DyTSPSi; 1TbTSPSi; 2DyTSPSi; 2TbTSPSi; 2′TbTSPSi; 3DyTSPSi)

0.26 mmol of hydrated $Ln(CH_3COO)$ (Ln = Dy(III) 0.088 g, Tb(III) 0.092 g) and 0.063 g of PhCOOH (0.52 mmol) were placed in a microwave reactor tube with 4 mL of a MeOH : MeCN mixture in 1:1 proportion. A pulse of 150 W is applied and the reaction kept for 10 minutes at a maximum temperature of 125 °C. The reaction is cooled to room temperature and a colorless precipitate is filtered. The colorless solution is diluted to 10 mL of MeCN : MeOH 1:1 and divided into vials. The **TSPSi** substrates in pieces of *ca.* 1×1 cm^2 were immersed into the solution and

kept for different times, from minutes to 24 h. The samples were removed from the reaction mixture, rinsed with MeOH, sonicated in MeOH and dried with N$_2$. Short deposition times (15 to 60 minutes) afforded **1DyTSPSi** and **1TbTSPSi** (typical values of thickness 2–6 nm, contact angle 68°). Longer deposition times (1 to 24 hours) afforded **2DyTSPSi** and **2TbTSPSi** (typical values of thickness 10–18 nm; contact angle 69°). Using a non-diluted reaction mixture, and an immersion time of 24 h we obtained a bulk-like sample, **3DyTSPSi** (thickness > 30 nm). This sample was rinsed but not sonicated. For terbium, using a non-diluted reaction mixture and with sample immersion of 1 h we obtained **2′TbTSPSi**.

Growth of $[Ln(CH_3COO)(PhCOO)_2]$ on Si(100) (1DySi, 1TbSi)

0.088 g (0.26 mmol) of hydrated $Dy(CH_3COO)$ and 0.063 g (0.52 mmol) of PhCOOH were placed in a microwave reactor tube with 4 mL of a MeOH : MeCN mixture in 1:1 proportion. A pulse of 150 W is applied and the reaction kept for 10 minutes at a maximum temperature of 125 °C. The reaction is cooled to room temperature and a colorless precipitate is filtered. The colorless solution is diluted to 10 mL of MeCN : MeOH 1:1 and divided into vials. The Si(100) was activated using piranha solution and rinsed. Immediately, Si(100) substrates in pieces of *ca.* 1×1 cm^2 were immersed into the diluted reaction solution and kept for 1 h (**1DySi**) and 24 h (**1TbSi**). The samples were removed from the reaction mixture, rinsed with MeOH and dried with N$_2$. Typical thickness was 2–10 nm. Contact angle values were 55–60°.

Characterization methods

The on-surface characterization of the lanthanoid 2D MOF layers on p-doped Si(100) substrates involved a variety of physicochemical techniques.

Contact angle measurements were carried out in a homemade instrument and analyzed with the ImageJ plugin DropSnake.[36] Ellipsometry data were collected with a J.A. Woollam Alpha-SE ellipsometer and analyzed with CompleteEase software. The beam diameter is <1 mm. For a typical sample, the thickness of the native SiO$_2$ layer was fitted using the SiO$_2$ relevant parameters in the CompleteEase software. Then, for the silane, the thickness was fitted using the parameters for an organic layer in CompleteEase software. For the samples containing a final layer of MOF, the thickness of the silane layer was subtracted from the thickness of the total organic layer obtained with CompleteEase software.

Scanning electron microscopy (SEM) images and energy dispersive X-ray spectroscopy (EDS) spectra were collected at the Unitat de Microscòpia Electrònica de Rastreig from Scientific and Technological Centers (CCiTUB), Universitat de Barcelona, using a Jeol J-6510 scanning electron microscope equipped with an EDS system and backscattered electron detector.

X-ray photoelectron spectroscopy (XPS) data were collected in the Anàlisi de Superficies unit from Scientific and Technological Centers (CCiTUB), Universitat de Barcelona, with a PHI

ESCA-5500 photoelectron spectrometer (X-ray source Al 1486.6 eV mono at 300.0 W).

Matrix assisted laser desorption ionization-time of flight (MALDI-ToF) mass spectroscopy experiments were performed at the Unitat d'Espectrometria de Masses de Caracterització Molecular from Scientific and Technological Centers (CCiTUB), Universitat de Barcelona. Cleaning of the samples was performed using a VWR USC600TH ultrasound cleaning bath at room temperature.

Luminescence of Tb 2D MOFs/TSP/Si samples was studied on a NanoLogTM-Horiba-Jobin Yvon iHR320 spectrophotometer using 280 nm excitation wavelength and the maximum opening of the slits (5 nm), with sample holder oriented at $45°$ to the incident beam and a front-face arrangement for the detector optics.

Atomic force microscopy (AFM) images were collected at CCITUB with a Bruker MultiMode 8-HR with Nanoscope V controller electronics in ScanAssist mode in air.

Hard X-ray photoelectron spectroscopy (HAXPES) data were collected under ultra-high vacuum ($P = 1 \times 10^{-10}$ mbar UHV) conditions using a photon energy of 12 keV at the BM25-SpLine beamline at the European Synchrotron ESRF. The diffraction data were collected using a massive S2D3 diffractometer equipped with a 2D detector, while the HAXPES data were obtained using a specially developed high kinetic energy analyzer, HV-CSA300, able to work up to kinetic energies of 15 keV.[37]

X-ray absorption spectroscopy (XAS) and X-ray magnetic circular dichroism (XMCD) measurements of nanometric Ln 2D MOFs deposited on surfaces were performed at BOREAS beamline of the ALBA synchrotron. We characterized **1LnTSPSi** (Ln = Dy, Tb), **2DyTSPSi** and **1DySi**. As a reference, XAS-XMCD measurements were also conducted on powdered $[Ln(CH_3COO)(PhCOO)_2]$ (Ln = Dy, Tb), pressed on an indium foil to ensure good thermal contact. Measurements across the $M_{4,5}$ edges of Dy(III) and Tb(III) were performed at $T = 3.4$ K $\pm$ 0.5 K. All spectra were recorded using Total Electron Yield (TEY) detection mode, with 90% circularly polarized light. The XMCD ($\mu^- - \mu^+$) and XAS ($\mu^+ + \mu^-/2$) spectra at 6 T were determined from at least eight X-ray absorption spectra measured under right-handed (μ^+) and left-handed (μ^-) circular polarizations. XMCD(H) cycles were performed by following the resonant M_5 peak while sweeping the magnetic field between 6 T and -6 T at a rate of 2 T min^{-1}. In addition, X-ray absorption spectroscopy under horizontal (H) and vertical (V) linear polarized light at the O K-edge was recorded to probe electronic anisotropy and formation of the chemisorbed 2D MOF material.

Magnetic properties of a bulk like (>30 nm) of Dy 2D MOF grafted on silanized Si (**3DyTSPSi**) were conducted using a Quantum Design MPMS SQUID equipped with a 5 T magnet at the SAI unit, Universidad de Zaragoza. The magnetic signal of the Ln 2D MOF was deduced after subtracting the **TSPSi** substrate contribution.

Author contributions

PS: conceptualization, methodology, investigation. GGR: investigation, validation. AA: investigation, formal analysis, data curation, writing: review and edit, visualization. JRZ: methodology, investigation. ECS: conceptualization, investigation, resources, data curation, visualization, supervision, project administration, funding acquisition, writing – original draft, review and editing. EB: investigation, resources, formal analysis, data curation, visualization, funding acquisition, writing – original draft, review and editing.

Conflicts of interest

There are no conflicts to declare.

Data availability

All relevant data are within the manuscript and its supplementary information (SI). Supplementary information: S1. Additional characterization of **1DyTSPSi** and **2DyTSPSi**; S2. XPS characterization of **1DyTSPSi**, **2DyTSPSi** and **3DyTSPSi**; S3. Additional magnetic characterization data. See DOI: https://doi.org/10.1039/d5tc02447a.

Acknowledgements

References

1 E. Coronado, *Nat. Rev. Mater.*, 2020, **5**, 87–104.

2 P. Miró, M. Audiffred and T. Heine, *Chem. Soc. Rev.*, 2014, **43**, 6537–6554.

3 E. Navarro-Moratalla, J. O. Island, S. Mañas-Valero, E. Pinilla-Cienfuegos, A. Castellanos-Gómez, J. Quereda, G. Rubio-Bollinger, L. Chirolli, J. Angel Silva-Guillén,

This journal is © The Royal Society of Chemistry 2025

J. Mater. Chem. C, 2025, **13**, 21015–21026 | **21025**

N. Agraït, G. A. Steele, F. Guinea, H. S. J. van der Zant and E. Coronado, *Nat. Commun.*, 2016, **7**, 1–7.

4 B. Huang, G. Clark, E. Navarro-Moratalla, D. R. Klein, R. Cheng, K. L. Seyler, D. Zhong, E. Schmidgall, M. A. McGuire and D. H. Cobden, *et al.*, *Nature*, 2017, **546**, 270–273.

5 J. Lobo-Checa, L. Hernández-López, M. M. Otrokov, I. Piquero-Zulaica, A. E. Candia, P. Gargiani, D. Serrate, F. Delgado, M. Valvidares, J. Cerdá, A. Arnau and F. Bartolomé, *Nat. Commun.*, 2024, **15**, 1858.

6 A. Urtizberea, E. Natividad, P. J. Alonso, M. A. Andrés, I. Gascón, M. Goldmann and O. Roubeau, *Adv. Funct. Mater.*, 2018, **28**, 1801695.

7 P. Konieczny, W. Sas, D. Czernia, A. Pacanowska, M. Fitta and R. Pełka, *Dalton Trans.*, 2022, **51**, 12762–12780.

8 F. Pointillart, B. Le Guennic, T. Cauchy, S. Golhen, O. Cador, O. Maury and L. Ouahab, *Inorg. Chem.*, 2013, **52**, 5978–5990.

9 J. H. Jia, Q. W. Li, Y. C. Chen, J. L. Liu and M. L. Tong, *Coord. Chem. Rev.*, 2019, **378**, 365–381.

10 J. González, P. Sevilla, G. Gabarró-Riera, J. Jover, J. Echeverría, S. Fuertes, A. Arauzo, E. Bartolomé and E. C. Sañudo, *Angew. Chem., Int. Ed.*, 2021, **60**, 12001–12006.

11 E. Bartolomé, A. Arauzo, S. Fuertes, L. Navarro-Spreafica, P. Sevilla, H. Fernández Cortés, N. Settineri, S. J. Teat and E. C. Sañudo, *Dalton Trans.*, 2023, **52**, 7258–7270.

12 G. Gabarró-Riera, G. Aromí and E. C. Sañudo, *Coord. Chem. Rev.*, 2023, **475**, 214858.

13 D. Gatteschi, A. Cornia, M. Mannini and R. Sessoli, *Inorg. Chem.*, 2009, **48**, 3408–3419.

14 G. Gabarró-Riera and E. C. Sañudo, *Commun. Chem.*, 2024, **7**, 99–110.

15 K. Katoh, H. Isshiki, T. Komeda and M. Yamashita, *Coord. Chem. Rev.*, 2011, **255**(17–18), 2124–2148.

16 E. Moreno Pineda, T. Komeda, K. Katoh, M. Yamashita and M. Ruben, *Dalton Trans.*, 2016, **45**, 18417–18433.

17 L. Tesi, A. Lunghi, M. Atzori, E. Lucaccini, L. Sorace, F. Totti and R. Sessoli, *Dalton Trans.*, 2016, **45**, 16635–16643.

18 I. Cimatti, L. Bondì, G. Serrano, L. Malavolti, B. Cortigiani, E. Velez-Fort, D. Betto, A. Ouerghi, N. B. Brookes, S. Loth, M. Mannini, F. Totti and R. Sessoli, *Nanoscale Horiz.*, 2019, **4**, 1202–1210.

19 K. Eguchi, Y. Takagi, T. Nakagawa and T. Yokoyama, *J. Phys. Chem. C*, 2014, **118**, 17633–17637.

20 L. Tesi, E. Lucaccini, I. Cimatti, M. Perfetti, M. Mannini, M. Atzori, E. Morra, M. Chiesa, A. Caneschi, L. Sorace and R. Sessoli, *Chem. Sci.*, 2016, **7**, 2074–2083.

21 V. Corradini, R. Biagi, U. Del Pennino, V. De Renzi, A. Gambardella, M. Affronte, C. A. Muryn, G. A. Timco and R. E. P. Winpenny, *Inorg. Chem.*, 2007, **46**, 4937–4943.

22 A. Ghirri, V. Corradini, V. Bellini, R. Biagi, U. Del Pennino, V. De Renzi, J. C. Cezar, C. A. Muryn, G. A. Timco, R. E. P. Winpenny and M. Affronte, *ACS Nano*, 2011, **5**, 7090–7099.

23 V. Corradini, A. Ghirri, E. Garlatti, R. Biagi, V. De Renzi, U. Del Pennino, V. Bellini, S. Carretta, P. Santini, G. Timco, R. E. P. Winpenny and M. Affronte, *Adv. Funct. Mater.*, 2012, **22**, 3706–3713.

24 J. A. J. Burgess, L. Malavolti, V. Lanzilotto, M. Mannini, S. Yan, S. Ninova, F. Totti, S. Rolf-Pissarczyk, A. Cornia, R. Sessoli and S. Loth, *Nat. Commun.*, 2015, **6**, 8216.

25 L. Rigamonti, M. Piccioli, L. Malavolti, L. Poggini, M. Mannini, F. Totti, B. Cortigiani, A. Magnani, R. Sessoli and A. Cornia, *Inorg. Chem.*, 2013, **52**, 5897–5905.

26 L. Malavolti, V. Lanzilotto, S. Ninova, L. Poggini, I. Cimatti, B. Cortigiani, L. Margheriti, D. Chiappe, E. Otero, P. Sainctavit, F. Totti, A. Cornia, M. Mannini and R. Sessoli, *Nano Lett.*, 2015, **15**, 535–541.

27 E. Bartolomé, A. Arauzo, S. Herce, A. Palau, N. Mestres, S. Fuertes, P. Sevilla, N. S. Settineri, L. Navarro-Spreafico, J. González and E. C. Sañudo, *Molecules*, 2021, **26**(18), 5503.

28 C. Haensch, S. Hoeppener and U. S. Schubert, *Chem. Soc. Rev.*, 2010, **39**, 2323–2334.

29 M. Sypabekova, A. Hagemann, D. Rho and S. Kim, *Biosensors*, 2023, **13**(1), 36.

30 L. Wang, U. S. Schubert and S. Hoeppener, *Chem. Soc. Rev.*, 2021, **50**, 6507–6540.

31 E. A. Smith and W. Chen, *Langmuir*, 2008, **24**, 12405–12409.

32 S. Kumar, G. G. Riera, A. Arauzo, J. Hrubý, S. Hill, L. Bogani, J. Rubio-Zuazo, J. Jover, E. Bartolomé and E. C. Sañudo, *J. Mater. Chem. A*, 2024, **12**, 6269–6279.

33 G. Gabarró-Riera, J. Jover, J. R. Zuazo, E. Bartolomé and E. C. Sañudo, *Inorg. Chem. Front.*, 2022, **9**, 4160–4170.

34 A. B. Altman, J. I. Pacold, J. Wang, W. W. Lukens and S. G. Minasian, *Dalton Trans.*, 2016, **45**, 9948–9961.

35 F. Frati, M. O. J. Y. Hunault and F. M. F. de Groot, *Chem. Rev.*, 2020, **120**, 4056–4110.

36 A. F. Stalder, G. Kulik, D. Sage, L. Barbieri and P. Hoffmann, *Colloids Surf.*, 2006, **286**, 92–103.

37 J. Rubio-Zuazo, M. Escher, M. Merkel and G. R. Castro, *Rev. Sci. Instrum.*, 2010, **81**, 043304.

21026 | *J. Mater. Chem. C*, 2025, **13**, 21015–21026

This journal is © The Royal Society of Chemistry 2025